NTU Journal for Renewable Energy (2025) Vol. 9 (1): 48-62
DOI: https://doi.org/10.56286/ntujre.v9i1

IRAQI Academic Scientific Journals

EISSN: 2788-9920
NTU Journal for Renewable Energy
Available online at:
https://journals.ntu.edu.iq/index.php/NTU-JRE

Modeling and Simulation of a PV-Induction Motor Water Pumping System for Off-Grid Irrigation

Saad M. Abdullateef[1], Zaki M. Abdullah[2], Bilal A. Nasir[3]

Northern Technical University

Article Information's

Received: 17 – 06 - 2025
Accepted: 20 – 08 - 2025
Published: 01 – 09 - 2025

Corresponding Author:
Saad M. Abdullateef

Email:
Saad.mutlaq411@gmail.com

Key words:
solar PV system, boost converter, 3-phase inverter, 3-phase induction motor, filter, water pumping system.

ABSTRACT

Solar-powered (PV) water pumping systems provide a sustainable and efficient solution for irrigation, especially in areas with high solar radiation and limited access to electrical grids. The performance of these systems depends on their ability to operate at the maximum power point (MPP) to ensure optimal energy extraction from solar panels. In this study, the Perturb and Observe (P&O) algorithm was used to track the maximum power point (MPPT), in addition, the scalar V/F technique to control the speed of a three-phase induction motor is implemented. The proposed system consists of a solar panel array, a DC-DC converter, a voltage inverter, an LC filter, and a water pump.

Meteorological data for the Kirkuk area (e.g., solar radiation & temperature) were incorporated into the system analysis to ensure that it is adapted to the local environmental conditions. The system was simulated using MATLAB/Simulink to evaluate the performance under variable environmental conditions. The results showed that the P&O algorithm provides effective MPP tracking, while the V/F control maintains the stability of the motor speed while minimizing energy loss. This system is recommended as an effective and low-cost solution for irrigation and water supply applications in remote areas with high solar radiation, such as Kirkuk, which has an average solar radiation of up to 5.5 kWh/m²/day and temperatures ranging from 10°C to 45°C, making it an ideal environment for solar energy systems.

INTRODUCTION

In recent decades, the scientific and technical community has paid close attention to environmental contamination and the growing global energy issues. Rapid advancements in fast-switching power electronics and semiconductor technology have significantly improved energy conversion techniques, leading to a rapid development in our understanding of how to transform renewable energy sources into usable forms. Renewable energy technology has advanced to the point that solar energy can now be directly converted into electrical energy, starting with the conversion of flowing water energy. Solar photovoltaic (PV) conversion systems used to be expensive and inefficient, with an efficiency of about 5% to 6% [1]. But as more research and technology advancements have been made, solar panels' efficiency has risen to 15–16%, and their price has steadily dropped. Since solar power conversion systems don't emit greenhouse gases or other harmful pollutants, don't require fuel, require little upkeep, and don't utilize water, they are now seen as a possible substitute for fossil fuel-based energy production systems. Nevertheless, this technology is still in its early stages of development, and issues including low efficiency, high initial cost, and intermittency need to be resolved.

The use of solar water pumps [2], [3] is growing in popularity in isolated and rural locations without power. In isolated locations, these systems are also favored for agricultural, water treatment, and irrigation applications. Solar pumping systems are seen to be the best way to increase agricultural output in Iraq, particularly in the Kirkuk region, where irrigation is a major component of agriculture. Solar pumping systems are more economical and environmentally friendly than diesel-powered systems, even though many water pumps worldwide are driven by electricity or non-renewable energy sources [4]. To maximize the quantity of energy generated and water pumped while overcoming the difficulties of working under changeable energy circumstances, innovative methods are needed when designing a motor system that runs directly from a solar energy source [5].

Because of their sturdy design, three-phase induction motors (IMD) perform well in solar pumping systems (SPS) when compared to other commercial motors. The development's objective is to provide solar water pumping systems that are economical, dependable, minimal maintenance, and efficient[6]. Despite their adoption in pumping applications, permanent magnet motors, such as brushless DC (BLDC) motors and sine wave motors, are still less popular than induction motors due to their higher cost and limited availability[7]. Additionally, induction motor production is at a mature level, which provides them a competitive edge for solar pumping applications in underdeveloped nations. Compared to conventional systems, induction motor-based pumping systems have seen significant improvements thanks to the use of advanced electronic switches, high-speed processors, and efficient motor control algorithms.

Pumping systems based on voltage source inverters (VSI) and induction motors connected to photovoltaic (PV) arrays have proven their operational efficiency. This study focuses on a three-phase induction motor-driven water pumping system designed to meet the needs of remote, off-grid communities. Despite the high initial cost of PV systems, subsequent efforts are focused on maximizing the utilization of energy generated by solar panels. Maximum power point tracking (MPPT) algorithms are essential in these systems, enabling the system to operate efficiently under variable irradiance conditions and extract the maximum available energy from the array. A few of these methods were examined in[8], and comparative research of several MPPT approaches has been given in [9][10].

Maximum power point tracking (MPPT) algorithms are a key component of solar energy systems. In this research, the Perturbation and Observation (P&O) method is used to determine the optimal operating point. This method involves inducing a sudden change in the solar array voltage and then monitoring the resulting change in output power to determine the optimal direction that leads to improved power extraction. The P&O approach is simple yet successful, especially under changing climatic circumstances. Compared with grid-connected systems[11] The fundamental problem with solar pumping systems is to properly regulate active power. This is due to the pump system's significantly larger mechanical time constant compared to other

systems. When solar irradiance declines abruptly, the voltage of the solar array drops dramatically, resulting in a fall in the flow level in the pump. Once the flow drops, the motor begins to draw more current, which can lead the motor to reach an unstable zone on the torque-speed curve, compromising the motor's health and diminishing system efficiency. As a result, MPPT algorithms should incorporate a method for dealing with these scenarios and restarting the motor as needed. Voltage-to-frequency (V/f) control method was used as a means to improve the performance efficiency of the three-phase induction motor within the proposed system. This technique is simple, straightforward to apply, and accessible [12][13]. Pumping applications have also made use of pumping systems based on VSI inverters and DC-DC converters[14][15]. Nevertheless, DC voltage instability affects these systems. On the other hand, V/f technology offers a more reliable and effective substitute.

In this research, the maximum power point (MPP) is tracked by adjusting the operating frequency, allowing the induction motor to extract the maximum available power from the solar panels, while maintaining constant torque under variable irradiance conditions. Compared to systems using DC motors, the proposed methodology demonstrates a higher water pumping capacity. Additionally, the V/f control technique improves the induction motor's start-up response in low irradiance conditions, enhancing the continuity and efficiency of the pumping process throughout the day. Real meteorological data from the Kirkuk region, including temperature and sun radiation, will be used in this study to enhance system performance and guarantee that it adapts to local environmental circumstances. With an average daily solar radiation of around 5.5 kWh/m2, the Kirkuk area is said to have significant solar potential and is therefore a perfect place to install solar pumping equipment.

1- DESIGN OF PROPOSED SYSTEM

The proposed solar water pumping system, as shown in Figure (1), consists of a photovoltaic (PV) array, a boost converter, a voltage source inverter (VSI), and a three-phase induction motor connected via a central LCL filter. The system includes a control unit that uses a maximum power point tracking (MPPT) algorithm, along with voltage/frequency (V/f) technology to adjust the motor's rotational speed. The PV array converts solar energy into direct current (DC) electrical energy, which is enhanced by a boost converter to ensure maximum power extraction even under fluctuating solar radiation. The VSI then converts the DC voltage to alternating current (AC) to power the motor and pump. The V/f control technology ensures that the voltage and frequency are proportional, enabling stable motor operation and precise speed regulation—both critical factors for achieving high water pumping efficiency. This system enhances performance efficiency and system reliability, making it particularly suitable for standalone solar-powered pumping applications.

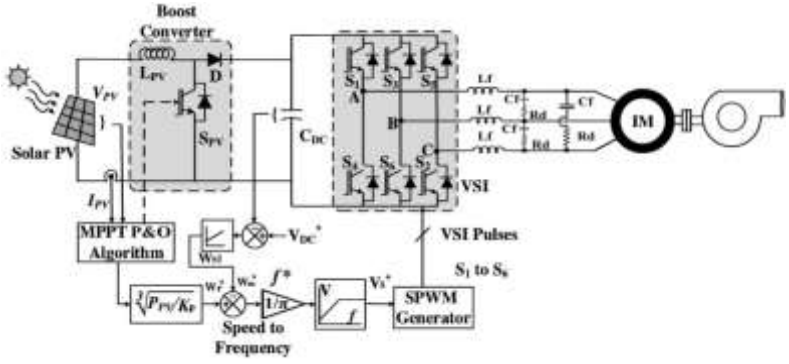

Figure (1) The PROPOSED SYSTEM

1.1 Maximum Power Point Tracking (MPTT) Algorithms

In recent decades, many maximum power point tracking (MPPT) methods, algorithms, and procedures have emerged in response to the trend towards developing more efficient and cost-effective solar energy systems. For even higher power output, several of the strategies, algorithms, and procedures have been improved. Numerous analyses and comparisons of MPPT approaches, algorithms, and procedures have been conducted [9] [16][17][18] [19][20][21]. To help us decide on this study, we provide an overview.

Subudhi and Pradhan [16] conducted a comprehensive analysis, identifying and categorising 26 unique MPPT approaches, algorithms, and procedures. They are classified based on a set of criteria, such as the number of control variables, types of control strategies, circuit design, cost, ease of

parameter tuning, level of complexity, along with the type of converter used (DC, AC, or both), as well as the nature of the application, whether it is a standalone system or grid-connected. Although these authors articulate significant observations regarding the suitability or unsuitability of specific approaches, algorithms, or methodologies, it is essential to recognise that the criteria for categorisation are general and possess a far wider applicability. The criteria are beneficial for selecting current and future MPPT techniques, algorithms, and procedures for certain applications. For instance, developing an MPPT methodology that employs voltage as the only control variable is more cost-effective than utilising current as the control variable.

Baba et al. [17] defined and analyzed a set of maximum power point tracking (MPPT) techniques, including perturbation and observation (P&O), incremental conductance (IC), constant voltage (CV), temperature dependence (T), open voltage (OV), and feedback voltage, as well as advanced algorithms such as fuzzy logic (FLC) and artificial neural networks (NN). The effectiveness of each technique was evaluated according to criteria including ease of implementation, associated cost, ability to identify multiple maximum power points, convergence speed, and efficiency over different output power ranges. The researchers concluded that the IC and P&O algorithms enable rapid tracking of the maximum power point while minimizing fluctuations around this point, thus improving the overall system output efficiency. These two methods were also ranked as the best options for MPPT applications in photovoltaic systems, due to their ease of implementation and role in reducing the system's cost payback period. According to Dollar et al. [22], both P&O and IC methods are similar in terms of cost and overall software requirements.

These results are consistent with those of Baba et al. [17], where the P&O and IC algorithms were found to be the most effective and feasible for implementing MPPT techniques in PV systems. It has recently been pointed out that both approaches are direct tracking methods, operating independently of solar radiation values, temperature, or degradation level, and can be implemented without prior knowledge of the PV system's current-voltage (I-V) curve[23].

Although the P&O and IC algorithms are widely used and highly appreciated, the incremental conductivity (IC) algorithm is more efficient in dynamic environments with rapid changes in radiation levels, as in these cases the P&O algorithm has shown relatively higher error rates [22].

1.2 The Solar Cell

Solar cells constitute the basis for photovoltaic panels or modules, which are subsequently employed to assemble photovoltaic arrays within photovoltaic systems. A solar cell is a two-terminal electronic component similar in characteristics to a light-emitting diode, converting photons from sunlight into electrical energy. **Figure (2)** shows the equivalent model of an analog circuit, which consists of a light current source, a semiconductor diode, a parallel resistor representing the leakage current, and a series resistor expressing the internal resistance to the flow of electric current. **Equation (1)** illustrates the I-V characteristic[24][25][26].

$$I = I_{ph} - I_0 \left[exp\left(\frac{q(V+R_S I)}{nKT}\right) - 1 \right] - \left[\frac{Vce+R_{sce}\, I}{pce}\right] \quad (1)$$

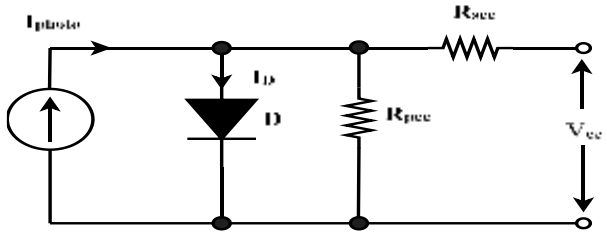

Figure (2) represents the equivalent circuit model for a photovoltaic solar cell

The symbol I_{ph} refers to the current resulting from light radiation (in amperes), and Io to the reverse saturation current (in amperes). R_{sce} represents the series resistance (in ohms), while R_{pce} represents the parallel resistance (in ohms). n is the diode coefficient, q is the electron charge and is equal to 1.6 × 10-19 coulombs, and K is the Boltzmann constant in units of joules/kelvin. T refers to the temperature of the solar panel (in kelvins), and V_{ce} to the output voltage from the cell.

Considering that the power produced by a solar cell, as indicated by the I-V curve in Equation (1), is rather low (about 45 mW), these cells are

interconnected in series or parallel to attain substantial electrical power for photovoltaic panel applications [27]. **Equation (1)** illustrates that the I-V curve for a photovoltaic cell is nonlinear and influenced by factors such as solar irradiation level, ambient temperature, wind speed, humidity, and pressure. This study examines the important parameters of irradiance and ambient temperature. In order to model and simulate the incremental conductivity (IC) algorithm, photovoltaic cell output data were initially obtained through practical modeling experiments. These experiments were conducted at a constant temperature of 25°C, with solar radiation intensity varying within a range of 400 to 1000 W/m². The results showed that the output current remained stable, while the voltage increased to a certain level and then began to decrease. **Table (1)** shows the technical specifications of the photovoltaic modules used in this study.

1.3 Design of Solar PV Array

The proposed system relies on an induction motor with a nominal power of 8.4 kW. Assuming losses from the motor and pump are neglected, the nominal power of the photovoltaic array must match the motor power to achieve the required energy balance. An 8.5-kW photovoltaic array is chosen in this instance.

The maximum power extracted from the solar array is calculated using the relationship:

$$P_{mp} = \left(N_p \times I_{mp}\right) \times \left(N_s \times V_{mp}\right) = 8.5 \text{ kW}$$

Where P_{mp} represents the maximum power that can be obtained from the solar panels at a given irradiance level, V_{mp} refers to the voltage at the maximum power point (MPP), and I_{mp} to the corresponding current. Ns and Np represent the number of modules connected in series and parallel, respectively. Considering that the open-circuit voltage of the solar panel is close to the DC link voltage, and taking into account that the required power is 8.5 kW, a configuration consisting of 8 modules connected in series and 2 modules in parallel was adopted. **Table (1)** shows the technical characteristics of both the individual solar module and the complete array.

Table (1) Characteristics and specifications of the PV Panel.

Parameter	**Value**
Peak power of the individual module	550 W
Open Circuit Voltage of the Module (V_{oc})	49. 9 V
Element short circuit current of the Module (I_{sc})	14 A
Element voltage at Maximum Power Point (Vmp)	41.9 V
Element current at Maximum Power Point (Imp)	13.13A
Array peak power (Pmp)	2.4 kW
Array open-circuit voltage (Voc)	459.69 V
Array short-circuit current (Isc)	7.13 A
Array voltage at Maximum Power Point (Vmp)	372.9 V
Array current at Maximum Power Point (Imp)	6.63 A

1.4 Design of The Boost Converter

The boost converter was selected because of its cost-effectiveness, ease of use, and efficiency. To ensure that the continuous conduction mode is maintained, the values of a few components, including the inductor and capacitor, were calculated using the appropriate formulae, whereas **Figure (3))** illustrates the fundamental circuit of an ideal boost converter with V_d and Vo serving as input and output voltages, respectively[25].

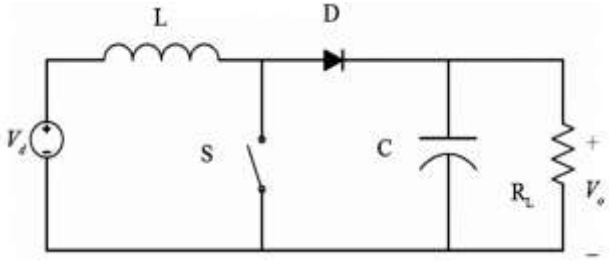

Figure (3) The ideal boost converter [25]

A boost converter can function in two distinct modes. The ON and OFF modes of the switch are the fundamental basis for its operation. Initially, as illustrated in **Figure (4)** , the charging situation transpires when the switch is closed. The switch will subsequently be activated to initiate the second operational mode, known as the discharge mode.

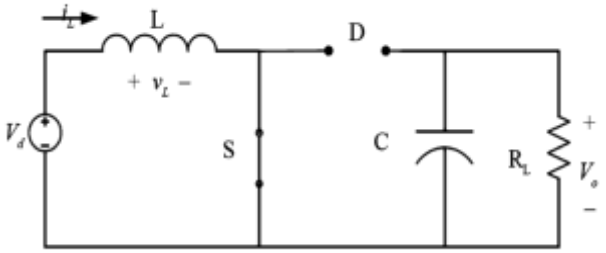

Figure (4) The equivalent circuit of the boost converter when switched to the closed position. [25]

$$V_d = V_l \quad (2)$$

$$V_d = L\frac{(I_{max}-I_{min})}{dt} \quad (3)$$

$$I_{max} = I_{min} + \frac{V_d}{L}dt \quad (4)$$

As shown in **Figure ()**, the switch is in the off state while the diode is in the forward bias state during the discharge phase. At this stage, the inductor discharges its stored energy into the capacitor, thus contributing to meeting the electrical load requirements. If the right amount of capacitor is employed, there is often very little ripple in the output load current and voltage.

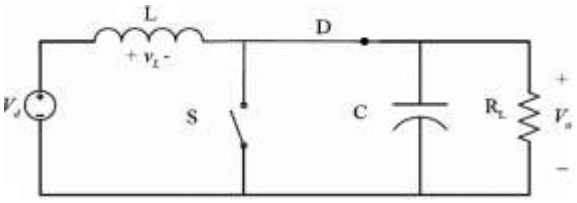

Figure (5) Equivalent circuit of the boost converter when the switch opened [25]

$$-V_d + V_L + V_0 = 0 \quad (5)$$

$$\frac{V_0}{V_d} = \frac{1}{1-d} \quad (6)$$

The **duty ratio** (D) of the converter can be calculated as[10]:

$$D = 1 - \frac{V_{in}}{V_{dc}} = 1 - \frac{335}{600} = 0.44 \quad (7)$$

The input capacitance (C_{in}), which is connected between the chopper and the solar PV arrays, and used as the input filter, can be calculated as [10]:

$$C_{in} \geq \frac{D^2}{V_{in}\times f_{sw}\times(1-D)\times(\Delta V_{dc}/V_{dc})} \quad (8)$$

ΔV_{dc} is selected to be equal (10% V_{dc}) = 10x600/100 = 60V

The boost converter switching frequency is assumed to be equal (10000) Hz

$$C_{in} \geq \frac{(0.44)^2}{335\times1000\times(1-0.44)\times(60/600)} \geq 1\mu F$$

The boost converter inductor can be calculated as[10]:

$$L_{boost} \geq \frac{V_{in}\times D}{\Delta I_L \times f_{sw}} \quad (9)$$

ΔI_L=current at maximum power×20% (ripple percent)

$$\Delta I_L = 0.2 \times 14.2 \times \sqrt{2} = 4A$$

$$L_{boost} \geq \frac{335 \times 0.44}{4 \times 10000} \geq 4\text{mH}$$

DC link capacity is a key component of the system, contributing to the stability of the required voltage during sudden changes in environmental conditions or rapid shifts in load requirements [10]:

$$C_{dc} \geq \frac{6\times\alpha\times V_{ph}\times I_{ph}\times t}{(V_{dc}^2 - V_{dc1}^2)} \quad (10)$$

Where:

α is the overloading factor = 1.2

V_{ph} is the r.m.s motor phase voltage = 400 V

I_{ph} is the r.m.s motor phase current = $I_L/\sqrt{3}$ = 14.2/√3 = 8.2 A

t is the recovery time of the minimum allowable DC link voltage (duration of transient) = 0.005 sec

The DC link capacitance C_{dc} is calculated as:

$$C_{\text{dc}} \geq \frac{6 \times 1.2 \times 400 \times 8.2 \times 0.005}{600^2 - 566^2} \geq 3000\mu F$$

The boost converter losses can be calculated in the same manner the same procedure and the same equations are used in the calculation of the inverter losses. When the loss equations calculated for the inverter are applied on a single MOSFET transistor switch, the following results are obtained:

The switching loss: $P_{sw} = 0.63$ W

The power loss in inductor resistance $= I^2_{dc} \times R_{boost} = (14.2)^2 \times 0.05 = 10$W

The conduction loss of the switch= 4.7 W

The conduction loss of the reverse diode= 4.7 W

Total losses= 0.63 + 10 + 4.7 + 4.7 = 20 W

The efficiency of the boost converter is equivalent to:

$\eta = P_{out} / P_{in} = 8600 / 8620 = 0.99 = 99.7\%$ (11)

1.5 The Filter Topology and Design

The output filter lowers the inverter switching-induced harmonics in the generated current. There are various kinds of filters. An L-filter, or inductor filter, attached to the inverter output is the simplest. Also, inductors and capacitors can be combined to create LC filters and LCL filters. **Figure (6)** illustrates the fundamental filter topologies [28].

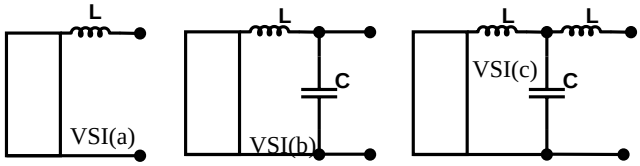

Figure (6) Basic Filter Topologies

The **L-filter depicted** in **Fig (6. a)** is a first-order filter exhibiting an attenuation of 20 dB per decade across the whole frequency spectrum. This filter is appropriate for inverters utilised in high switching frequency applications.

The **LC filter** in **Fig (6. b)** is a second-order filter and has better damping behavior than the L filter.

The **LCL** filter shown in **Fig (6.c)** is a third-order filter, with an attenuation capacity of up to 60 dB per frequency decade, within the range between the resonant frequency and the switching frequency of the inverter. Additionally, it reduces current ripple across the load inductance and improves decoupling between the filter and the motor load. This LCL filter is compatible with the induction motor-solar PV inverter system. Therefore, an LCL filter must be carefully designed and modeled to meet the requirements of the overall system. This filter is installed between the inverter output and the load, represented by the induction motor, to reduce harmonics resulting from the inverter's non-ideal output voltage. Since the inverter output waveform is not perfectly sinusoidal, it becomes necessary to use an LCL low-pass filter and connect it between the inverter and the motor, as shown in **Figure (1).**

First, the base impedance or characteristic impedance of the filter needs to be calculated, which is used to calculate the filter components as [29]:

$$Z_{\text{base}} = \frac{V^2_{\text{Inv/ph.}}}{S_{\text{Inv/ph.}}} = \frac{(\text{inverter output phase voltage r.m.s})^2}{(\text{inverter output apparent power per phase})} \quad (12)$$

$$S_{\text{inv/ph}} = V_{\text{inv/ph}} \times I_{\text{inv/ph}} = 400 \times \frac{14.2}{\sqrt{3}} = 3279.5 \text{ VA} \quad (13)$$

$$Z_b = \frac{(400)^2}{3279.5} = 48.8\Omega$$

The base capacitance (C_b) is determined as:

$$C_b = \frac{1}{\omega_s \cdot Z_b} = \frac{1}{2\pi \cdot 50 \cdot 48.8} = 65\mu\text{F} \quad (14)$$

Where ω_s is the angular frequency of the load.

The determination of the filter capacitor capacitance is based on the principle that the maximum permissible variation in power factor does not exceed 5% of the nominal surface power per phase (5% of Sph). The capacitance of the capacitor cf can be calculated by multiplying the system base capacitance Cb by 0.05, as shown in the following relationship [29]:

$$C_f = 0.05 \times C_b = 0.05 \times 65 = 3.3\mu F \quad (15)$$

The output current ripple can be estimated to be 10% of the nominal current by calculating the

inverter output inductance value L_{inv}, which is calculated according to the following equation:

$$L_{\text{inv}} = \frac{V_{\text{DC}}}{6 \cdot f_{\text{sw}} \cdot \Delta I_{\text{ph(max)}}} = 1.15\text{mH} \quad (16)$$

$$\text{where } \Delta I_{\text{ph(max)}} = 25\% \cdot \left(\frac{I_L}{\sqrt{3}}\right) \cdot \sqrt{2} = 0.25 \cdot 8.2 \cdot \sqrt{2} = 2.9A$$

The filter inductance on the motor side can be considered negligible, as its value is small compared to the leakage inductance in both the stator and rotor.

The capacitor Cf should be connected in series with a resistance, which is called damping resistance (Rd), which can be calculated as [29]:

$$R_d = \frac{1}{3\,\omega_{res}\,C_f} = 5.7\ \Omega \quad (17)$$

Where ω_{res} is the resonance angular frequency.

The DC link voltage must exceed the maximum line voltage of the induction motor:

$V_{dc(max)} = \sqrt{2} \times 400 = 566\,Volts$, This value represents the minimum allowable DC voltage. The DC voltage can be used as the output voltage of the boost converter and is fixed at 600 volts to ensure stable operation. Therefore, 566 volts is the minimum acceptable DC voltage.

1.6 Design of Centrifugal Pump Model

Both volumetric and centrifugal pumps are used in photovoltaic (PV)-based water pumping systems [30]. However, studies have shown that centrifugal pumps consume relatively more energy from the PV generator than volumetric pumps. This difference is attributed to the ability of centrifugal pumps to operate for extended periods, even in low solar radiation conditions, and their load curve matches the maximum power point (MPP) of the solar generator. These pumps are characterized by their low cost, ease of operation, low maintenance requirements, and availability in a variety of flow rates and pressures. The process of selecting a suitable centrifugal pump model for use in this project is currently underway.

The proportionality constant (K_{pump}) of a given water pump is calculated according to the following relationship:

$$K_{pump} = \frac{T_L}{\omega_r^2} \quad (18)$$

The load torque of a water pump, T_L, is equal to the torque of an induction motor during steady-state operation, and the rotor's rotational speed, ωr, is expressed in radians per second. The rated torque and speed of the induction motor are 50 N-m and 1430 rpm, respectively. The proportionality constant (Kpump) is determined using equation (12) as follows:

$$K_{pump} = \frac{50}{\left(2\pi \times \frac{1430}{60}\right)^2} = 0.0022\ \ N \cdot m/(rad/s)^2$$

So, the proportionality constant is selected as 0.0022 N.m/(r/s).

2- CONTROL SCHEME DESIGN FOR THE PROPOSED SYSTEM

Figure (1) shows the proposed system configuration, which relies on a two-stage structure to regulate the water pumping process using solar photovoltaic energy. The first stage focuses on applying the maximum power point tracking (MPPT) algorithm using the disturbance and observation (P&O) method to enhance the efficiency of energy extraction from the solar array. This method is popular due to its simplicity and ease of implementation, as it relies on gradually adjusting the operating voltage and observing the change in the resulting power. If the power increases, the change is maintained in the same direction, while if it decreases, the direction is reversed. This process is repeated continuously to track the optimal operating point. However, it may lead to fluctuations around the maximum power point, especially under rapidly changing environmental conditions.

The second stage focuses on regulating the speed of the input motor through voltage-to-frequency ratio (V/F Control) technology. This approach preserves a consistent ratio between voltage and frequency to effectively regulate motor speed. Voltage/frequency control is preferred for its simplicity, unlike more complex control systems, such

as field-oriented control (FOC) and direct torque control (DTC), which require intensive calculations. Moreover, executing these algorithms in a sensor-free environment introduces complexity owing to the challenges associated with indirect speed estimation and other operational parameters.

Both the voltage and current generated by the photovoltaic array are monitored and fed into a disturbance and monitoring (P&O) algorithm, which analyzes changes in electrical parameters such as voltage, current, and power to determine the appropriate duty cycle for the boost converter. A proportional-integral (PI) controller is used to maintain the boost converter's output voltage at a constant reference level, ensuring stable power supply to the inverter and induction motor. Due to the dynamic nature of the centrifugal pump, there is a direct relationship between the power consumed and the motor's rotational speed. The speed feed-forward rate can be estimated based on the available power from the photovoltaic cells, reducing the system's dependence on the PI controller's output while simultaneously improving the system's dynamic response.

Regarding inverter control, the voltage/frequency (V/F) technology generates the switching logic for the voltage source inverter (VSI) using sinusoidal pulse width modulation (SPWM). When the DC-link voltage exceeds a specified reference value, the PI controller increases the reference speed used in the control system. V/F, while this speed decreases if the voltage drops below the reference value. Combining the feedforward signal with the PI controller outputs produces a speed reference signal (f)*, which is subsequently used as an input to the induction motor's (IMD) V/F control algorithm.

a) Perturb and observe (P&O) algorithm

Due to its simple structure and ease of implementation, the Perturbation and Observe (P&O) algorithm is one of the most widely used maximum power point tracking (MPPT) techniques. This algorithm is based on the assumption that the change in the output power of a photovoltaic array on the power versus voltage curve is zero (ΔPPV) at the maximum power point, as shown in the **Figure (7))** [31,32,33,34]. The PV array terminal voltage or current is regularly perturbed (incremented or decremented) by the P&O, which then compares the resulting output power of the PV array P(n+1) with that at the previous perturbation (n). If a perturbation in terminal voltage leads to an increase in PV power (ΔPPV > 0), keep the perturbation in the same direction. Otherwise, move the perturbation to the other direction. The perturbation cycle is continued until the maximum power is achieved (ΔPPV = 0). **Figure (**8)) shows the P&O control flow chart. There are two alternative approaches to implementing the P&O algorithm. Traditionally, a reference voltage is utilized as a perturbation parameter; hence, a PI controller is required to modify the duty ratio[33][35][36]. The second method is to directly disrupt the duty ratio and measure the power for each PWM cycle [32][37]. This approach has the benefit of being simple, easy to execute, and does not require a prior understanding of the PV array. However, once the MPP is reached, the P&O will continue to disturb and wobble about it, resulting in some wasteful power loss[38].

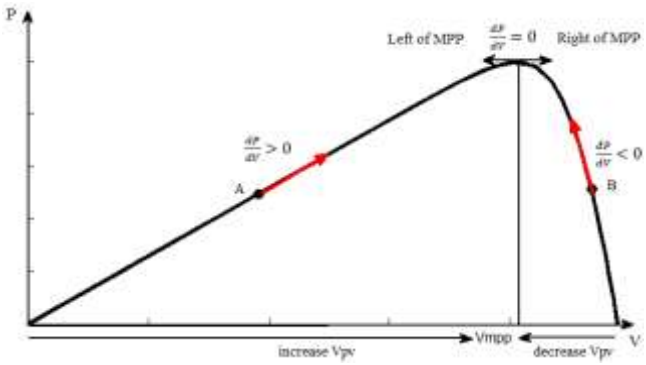

Figure (7) Sign of the dP/dV at different positions on the power characteristic.

b) Scalar (V/f) Control of Induction Motor

Scalar control of an induction motor is the most used and simplest control technique to date. Induction motors are often designed for a 50 Hz input voltage. The voltage must be decreased to allow for lower-speed operation. Constant flux operation requires frequency control as well as voltage magnitude control. The voltage should be proportional to the frequency such that the flux magnitude remains constant ($\psi s=V/\omega$). An IM is typically supplied by a three-phase PWM VSI[39-45]. The reference speed is only one of the input parameters. Neglecting the minor slip speed, the motor's speed is about equal to

the reference speed. The speed reference is integrated to get the θ, which is utilized to obtain three sinusoidal voltage references. The voltage references are compared with high-frequency triangular waves to generate the switching pulses required to operate the voltage source inverter (VSI). The speed reference is evaluated using the control mechanism shown in Figure (1).

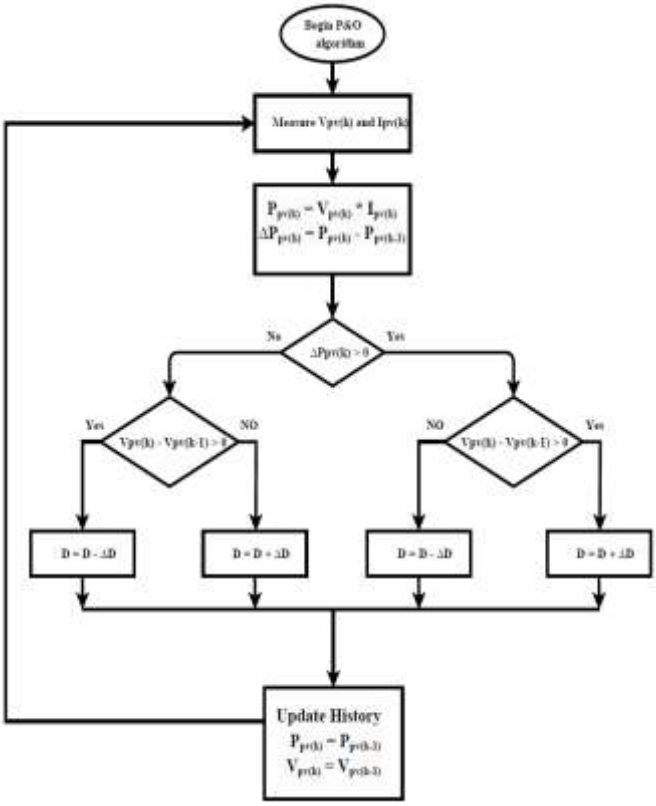

Figure (8) The P&O Algorithm Flowchart

The maximum reference voltage for the induction motor output (Vs) is calculated within the V-F control block according to the relationship shown in the same figure:

$$V_s^* = \frac{(V_{rated} - V_\circ)}{(f_{rated} - f_\circ)} + V_\circ \qquad (13)$$

$$V_\circ = I_{ph} * R_s \qquad (14)$$

Where V_{rated} is the rated maximum phase voltage of the motor.

$V_\circ$ is the voltage drop across each phase of the motor, f_{rated} is the rated frequency of the motor and $f_\circ$ is the frequency corresponding to the voltage drop ($V_\circ$).

$$\theta = \int \omega^* \, dt \qquad (19)$$

The three-phase reference voltages are as:

$$V_a^* = M_a \times V_s^* \, sin(\theta) \qquad (20)$$

$$V_b^* = M_a \times V_s^* \, sin(\theta - 120^\circ) \qquad (21)$$

$$V_c^* = M_a \times V_s^* \, sin(\theta - 240^\circ) \qquad (22)$$

Where,

$M_a = f_s^*/f_{rated}$ *is the modulation index*

RESULTS AND DISCUSSION

The simulation environment is used to evaluate the performance of a photovoltaic-powered multistage water pumping system. The proposed model was developed and implemented using the MATLAB/Simulink platform for dynamic modeling and analysis. To verify the system's efficiency under varying operating conditions, a simulation of gradual changes in solar radiation levels was included.

The complete structure of the proposed system is illustrated in Figure (9), which includes the photovoltaic (PV) array, DC-DC boost converter, fuzzy-based MPPT controller, voltage and current sensors, voltage regulator, three-phase inverter, V/F controller, induction motor, and the water pump.

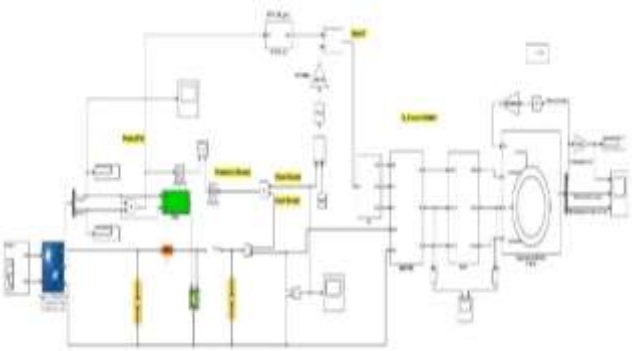

Figure (9): Block diagram of the proposed photovoltaic-powered water pumping system.

Case 1: Starting performance under Constant Irradiance at 1000 W/m²

Figure (10) Rotor Speed, Stator Current, and Electromagnetic Torque

Under constant solar irradiance of 1000 W/m², in Figure (10), the rotor speed smoothly increases and stabilizes around 1430 rpm. The stator current initially shows transient oscillations due to the motor startup phase, then stabilizes with a symmetrical waveform. The electromagnetic torque starts with fluctuations and settles around 45 Nm, indicating a balanced motor operation.

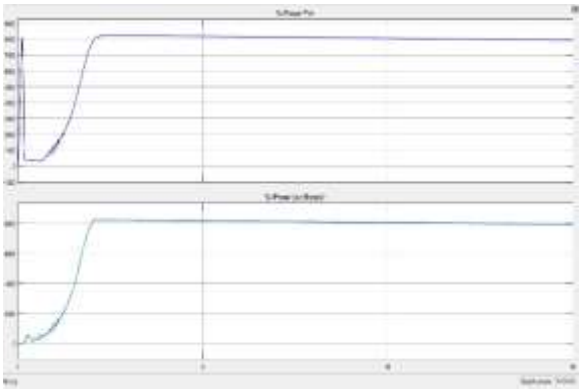

Figure (11) PV Power and Boost Output Power

The PV power in Figure (11), rapidly reaches its peak around 8500 W and remains constant, showing that the MPPT algorithm effectively extracted the maximum power under stable irradiance. The power after the boost converter mirrors this behavior, demonstrating minimal The output voltage of the boost converter in Figure (12), quickly rises and stabilizes near 600 V. The output current remains steady after the initial surge. This stability confirms the effectiveness of the voltage control loop in maintaining a regulated DC output despite initial transients.

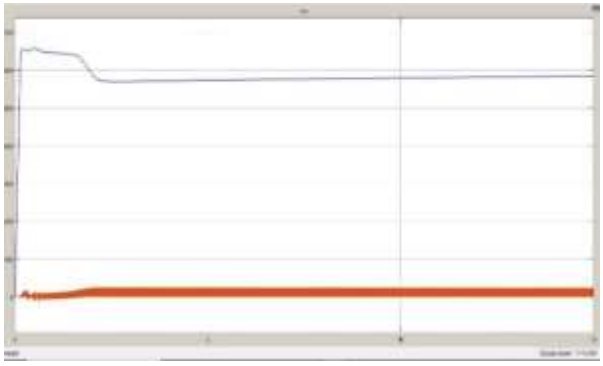

Figure (12) Output Voltage and Current of Boost Converter

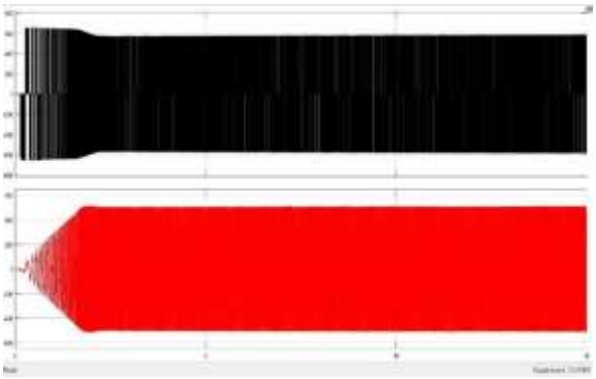

Figure (13) Inverter Output Voltage before and after Filter

The inverter output voltage in Figure (13), before filtering, contains high-frequency switching harmonics, which are effectively eliminated by the filter. The filtered voltage exhibits a clean sinusoidal waveform, confirming the filter's role in providing a stable three-phase voltage to the induction motor.

Furthermore, the voltage before and after filtering was analyzed using the Fourier series transform. The results, as illustrated in the harmonic spectrum in Figure (14), showed that the Total Harmonic Distortion (THD) of the voltage supplied to the induction motor is 5.88%, which is within the acceptable limits defined by the IEEE standard, thereby confirming the system’s compliance with power quality requirements.

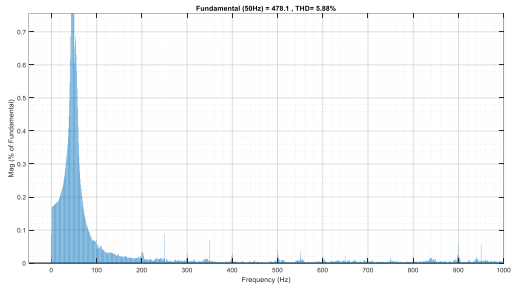

Figure (14): Harmonic spectrum of inverter output voltage after filtering showing THD = 5.88%

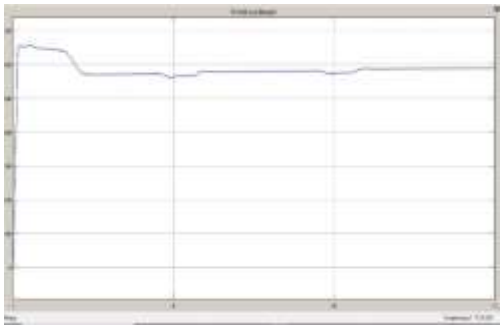

Figure (15) Output Voltage of Boost Converter

As the irradiance in Figure (15) changes at t = 5s (1000 to 700 W/m^2) and t = 10s (700 to 500 W/m^2), the boost converter output voltage experiences slight dips but quickly recovers and stabilizes around new values (~600V and ~580V, respectively). This indicates the controller's resilience in dynamically adjusting to varying input power levels.

Case 2: Variable Irradiance (1000 W/m² → 700 W/m² → 500 W/m²)

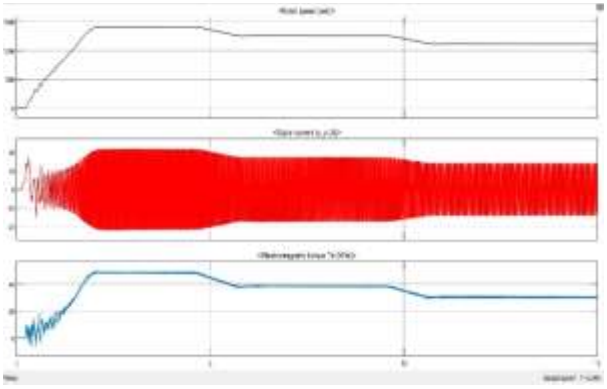

Figure (16) Rotor Speed, Stator Current, and Electromagnetic Torque

The rotor speed in Figure (16) decreases at t = 5s and again at t = 10s, corresponding to the drop in solar irradiance. The stator current amplitude reduces accordingly, and the electromagnetic torque experiences slight drops. Despite these variations, the system remains operational and dynamically stable.

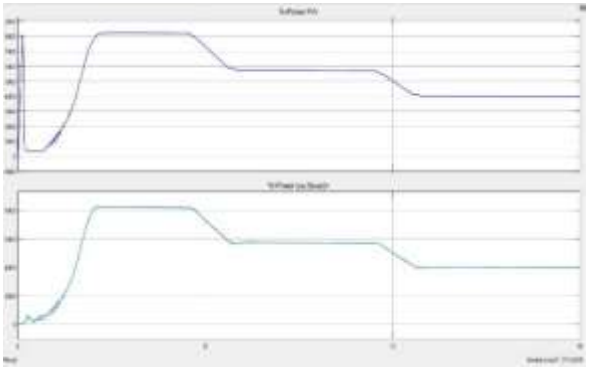

Figure (17) PV Power and Boost Output Power

Both PV power and output power after the boost converter in Figure (17) decrease in steps at t = 5s and t = 10s, directly reflecting the reduction in available solar energy. However, the transitions are smooth, indicating the MPPT and boost control maintain good performance under irradiance variation.

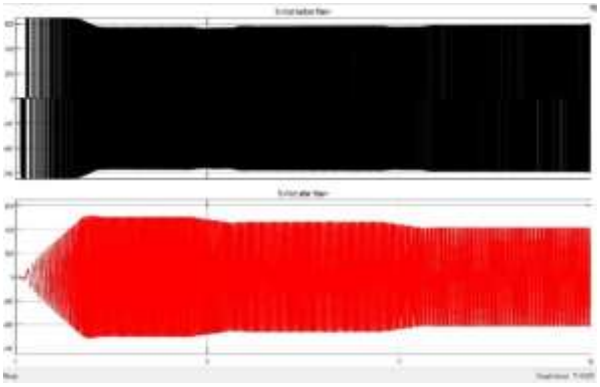

Figure (18) Inverter Output Voltage before and after Filter

The inverter output voltage shown in Figure (18) demonstrates minor variations in magnitude during the irradiance transitions observed at t = 5s and t = 10s. Despite these fluctuations, the filtered waveform maintains its sinusoidal shape, ensuring reliable and steady operation of the induction motor under dynamic input conditions.

COMPARATIVE ANALYSIS AND CONCLUSION

The simulation results under both constant and variable irradiance conditions demonstrate the effectiveness and robustness of the proposed control strategy. Under constant irradiance (1000 W/m²), the system operates with high stability in all key parameters: voltage, power, speed, and torque. The MPPT algorithm consistently extracts maximum power, and the boost converter maintains a regulated voltage, enabling efficient motor operation. The inverter supplied clean three-phase voltage to the induction motor, which achieved smooth startup and stable speed and torque without exceeding current limits.

In the variable irradiance scenario (1000 → 700 → 500 W/m²), the system adapts smoothly to irradiance changes at t = 5s and t = 10s. Although slight dips in voltage, power, and torque are observed, the control loops respond quickly stabilize the system, and adjust dynamically to reduced power input, maintaining voltage regulation and sinusoidal motor supply. Although motor speed and torque declined proportionally with irradiance, system stability, and functionality were preserved throughout. This proves the controller's capacity to handle real-world environmental fluctuations. Overall, the integration of MPPT, voltage regulation, and V/F speed control ensures the reliable performance of the solar water pumping system. The comparison results highlight that constant solar radiation achieves optimal performance under stable operating conditions, while the system demonstrates high flexibility and reliability when faced with environmental fluctuations, confirming its suitability for practical applications in real-world environments.

Simulation results demonstrate the efficiency and reliability of the proposed multi-level control structure in adapting to both stable and variable solar radiation conditions. This design proves suitable for practical deployment in standalone PV-based agricultural water pumping systems. Future work will focus on experimental implementation and the integration of energy storage or hybrid sources to enhance performance during prolonged low-irradiance periods.

References

[1] E. Drury, T. Jenkin, and D. Jordan, "Photovoltaic Investment Risk and Uncertainty for Residential Customers," *Photovoltaics, IEEE J.*, vol. 4, pp. 278–284, Jan. 2014, doi: 10.1109/JPHOTOV.2013.2280469.

[2] Muljadi, "PV water pumping with a peak-power tracker using a simple six-step square-wave inverter," *IEEE Trans. Ind. Appl.*, vol. 33.3, pp. 714–721, 1997.

[3] E. de Santana, J. Jesus Fiais Cerqueira, and T. Silva Flanklin, "Fuzzy and PI controllers in pumping water system using photovoltaic electric generation," *IEEE Lat. Am. Trans.*, vol. 12, no. 6, pp. 1049–1054, 2014, doi: 10.1109/TLA.2014.6893999.

[4] R. Kumar and B. Singh, "BLDC Motor-Driven Solar PV Array-Fed Water Pumping System Employing Zeta Converter," *IEEE Trans. Ind. Appl.*, vol. 52, no. 3, pp. 2315–2322, 2016, doi: 10.1109/TIA.2016.2522943.

[5] S. Jain, A. K. Thopukara, R. Karampuri, and V. T. Somasekhar, "A Single-Stage Photovoltaic System for a Dual-Inverter-Fed Open-End Winding Induction Motor Drive for Pumping Applications," *IEEE Trans. Power Electron.*, vol. 30, no. 9, pp. 4809–4818, 2015, doi: 10.1109/TPEL.2014.2365516.

[6] J. Caracas, G. Farias, L. Teixeira, and L. Ribeiro, "Implementation of a High-Efficiency, High-Lifetime, and Low-Cost Converter for an Autonomous Photovoltaic Water Pumping System," *Ind. Appl. IEEE Trans.*, vol. 50, pp. 631–641, Jan. 2014, doi: 10.1109/TIA.2013.2271214.

[7] R. Antonello, M. Carraro, A. Costabeber, F. Tinazzi, and M. Zigliotto, "Energy-Efficient Autonomous Solar Water-Pumping System for Permanent-Magnet Synchronous Motors," *IEEE Trans. Ind. Electron.*, vol. 64, no. 1, pp. 43–51, 2017, doi: 10.1109/TIE.2016.2595480.

[8] M. Calavia, J. Perié, J. Sanz, and J. Sallán, *Comparison of MPPT strategies for solar modules*. 2010.

[9] T. Esram and P. L. Chapman, "Comparison of Photovoltaic Array Maximum Power Point Tracking Techniques," *Energy Conversion, IEEE Trans.*, vol. 22, pp. 439–449, Jul. 2007, doi: 10.1109/TEC.2006.874230.

[10] A. Garrigós, J. M. Blanes, J. A. Carrasco, and J. B. Ejea, "Real-time estimation of photovoltaic modules characteristics and its application to maximum power point operation," *Renew. Energy*, vol. 32, no. 6, pp. 1059–1076, 2007, doi: https://doi.org/10.1016/j.renene.2006.08.004.

[11] B. Singh, S. Kumar, and C. Jain, "Damped-SOGI-Based Control Algorithm for Solar PV Power Generating System," *IEEE Trans. Ind. Appl.*, vol. 53, no. 3, pp. 1780–1788, 2017, doi:

10.1109/TIA.2017.2677358.
[12] X.-D. Sun, K.-H. Koh, B.-G. Yu, and M. Matsui, "Fuzzy-Logic-Based V/f Control of an Induction Motor for a DC Grid Power-Leveling System Using Flywheel Energy Storage Equipment," *IEEE Trans. Ind. Electron.*, vol. 56, no. 8, pp. 3161–3168, 2009, doi: 10.1109/TIE.2009.2021679.
[13] S. R. Bhat, A. Pittet, and B. S. Sonde, "Performance Optimization of Induction Motor-Pump System Using Photovoltaic Energy Source," *IEEE Trans. Ind. Appl.*, vol. IA-23, no. 6, pp. 995–1000, 1987, doi: 10.1109/TIA.1987.4505020.
[14] Y. Yao, P. Bustamante, and R. S. Ramshaw, "Improvement of induction motor drive systems supplied by photovoltaic arrays with frequency control," *IEEE Trans. Energy Convers.*, vol. 9, no. 2, pp. 256–262, 1994, doi: 10.1109/60.300150.
[15] F. Karbakhsh, M. Amiri, and H. Zarchi, "Two-switch flyback inverter employing a current sensorless MPPT and scalar control for low cost solar powered pumps," *IET Renew. Power Gener.*, vol. 11, Nov. 2016, doi: 10.1049/iet-rpg.2016.0631.
[16] B. Subudhi and R. Pradhan, "A Comparative Study on Maximum Power Point Tracking Techniques for Photovoltaic Power Systems," *IEEE Trans. Sustain. Energy*, vol. 4, no. 1, pp. 89–98, 2013, doi: 10.1109/TSTE.2012.2202294.
[17] S. Babaa, M. Armstrong, and V. Pickert, "Overview of Maximum Power Point Tracking Control Methods for PV Systems," *J. Power Energy Eng.*, vol. 02, pp. 59–72, Jan. 2014, doi: 10.4236/jpee.2014.28006.
[18] N. Femia, G. Lisi, G. Petrone, G. Spagnuolo, and M. Vitelli, "Distributed maximum power point tracking of photovoltaic arrays: Novel approach and system analysis," *IEEE Trans. Ind. Electron.*, vol. 55, no. 7, pp. 2610–2621, 2008, doi: 10.1109/TIE.2008.924035.
[19] R. Faranda and S. Leva, "Energy comparison of MPPT techniques for PV Systems," *J. Electromagn. Anal. Appl.*, vol. 3, Jan. 2008.
[20] D. Sera, T. Kerekes, R. Teodorescu, and F. Blaabjerg, "Improved MPPT method for rapidly changing environmental conditions," in *2006 IEEE International Symposium on Industrial Electronics*, 2006, pp. 1420–1425. doi: 10.1109/ISIE.2006.295680.
[21] N. Femia, G. Petrone, G. Spagnuolo, and M. Vitelli, "Optimization of perturb and observe maximum power point tracking method," *IEEE Trans. Power Electron.*, vol. 20, no. 4, pp. 963–973, 2005, doi: 10.1109/TPEL.2005.850975.
[22] A. Dolara, "Energy comparison of seven MPPT techniques for PV systems," *J. Electromagn. Anal. Appl.*, vol. 01, pp. 152–162, Jan. 2009, doi: 10.4236/jemaa.2009.13024.
[23] D. Baimel, S. Tapuchi, and N. Baimel, "New Improved Maximum Power Point Tracking Algorithm for Partially Shaded PV Systems," *J. Power Energy Eng.*, vol. 05, pp. 55–63, Jan. 2017, doi: 10.4236/jpee.2017.59005.
[24] D. A. Asoh, B. D. Noumsi, and E. N. Mbinkar, "Maximum Power Point Tracking Using the Incremental Conductance Algorithm for PV Systems Operating in Rapidly Changing Environmental Conditions," *Smart Grid Renew. Energy*, vol. 13, no. 05, pp. 89–108, 2022, doi: 10.4236/sgre.2022.135006.
[25] I. B. Ezugwu, O. Comfort, and B. Noumsi, "Simulation of A Modified Perturb and Observe Algorithm for A Photovoltaic System Connected To the Grid," vol. 5, pp. 1052–1059, May 2019.
[26] C. Aissa, S. Silvestre, N. Sadaoui, and R. Lazhar, "Modeling and simulation of a grid-connected PV system based on the evaluation of main PV module parameters," *Simul. Model. Pract. Theory*, vol. 20, pp. 46–58, Jan. 2012, doi: 10.1016/j.simpat.2011.08.011.
[27] K. Khan, S. Shukla, and B. Singh, "Performance-Based Design of Induction Motor Drive for Single-Stage PV Array Fed Water Pumping," *IEEE Trans. Ind. Appl.*, vol. 55, no. 4, pp. 4286–4297, 2019, doi: 10.1109/TIA.2019.2910484.
[28] A. Reznik, M.G. Simões, A. Al-Durra, & S. M. Muyeen, "LCL filter design and performance analysis for grid-interconnected systems," IEEE Transactions on Industry Applications, 50(2), pp.1225-1232,2013.
[29] A.E.W.H. Kahlane, L. Hassaine, and M. Kherchi, " LCL filter design for photovoltaic grid-connected systems", Revue des Energies Renouvelables SIENR'14 Ghardaïa, pp. 227 – 232, 2014.
https://www.cder.dz/download/sienr2014_31.pdf
[30] A. Mokeddem, A. Midoun, D. Kadri, S. Hiadsi, and I. Raja, "Performance of a directly-coupled PV water pumping system," *Energy Convers. Manag. - ENERG CONV Manag.*, vol. 52, pp. 3089–3095, Sep. 2011, doi: 10.1016/j.enconman.2011.04.024.
[31] E. Koutroulis, K. Kalaitzakis, and N. C. Voulgaris, "Development of a microcontroller-based, photovoltaic maximum power point tracking control system," *IEEE Trans. Power Electron.*, vol. 16, no. 1, pp. 46–54, 2001, doi: 10.1109/63.903988.
[32] F. Liu, Y. Kang, Y. Zhang, and S. Duan, "Comparison of P&O and hill climbing MPPT methods for grid-connected PV converter," in *2008 3rd IEEE Conference on Industrial Electronics and Applications*, 2008, pp. 804–807. doi: 10.1109/ICIEA.2008.4582626.
[33] P. L. and R. R., "Adaptive perturb and observe algorithm for photovoltaic maximum power point tracking," *IET Renew. Power Gener.*, vol. 4, no. 4, pp. 317–328, Jul. 2010, doi: 10.1049/iet-rpg.2009.0006.
[34] C. Jaen, C. Moyano, X. Santacruz, J. Pou, and A. Arias, "Overview of maximum power point

tracking control techniques used in photovoltaic systems," in *2008 15th IEEE International Conference on Electronics, Circuits and Systems*, IEEE, 2008, pp. 1099–1102.

[35] W. Xiao and W. G. Dunford, "A modified adaptive hill climbing MPPT method for photovoltaic power systems," in *2004 IEEE 35th Annual Power Electronics Specialists Conference (IEEE Cat. No.04CH37551)*, 2004, pp. 1957-1963 Vol.3. doi: 10.1109/PESC.2004.1355417.

[36] C. Hua and C. Shen, "Study of maximum power tracking techniques and control of DC/DC converters for photovoltaic power system," in *PESC 98 Record. 29th Annual IEEE Power Electronics Specialists Conference (Cat. No.98CH36196)*, 1998, pp. 86–93 vol.1. doi: 10.1109/PESC.1998.701883.

[37] C. W. Tan, T. C. Green, and C. A. Hernandez-Aramburo, "Analysis of perturb and observe maximum power point tracking algorithm for photovoltaic applications," in *2008 IEEE 2nd International Power and Energy Conference*, 2008, pp. 237–242. doi: 10.1109/PECON.2008.4762468.

[38] S. Gupta, O. Singh, and M. A. Ansari, "Maximum power point tracking techniques for the photovoltaic system: A review," *Lect. Notes Electr. Eng.*, vol. 526, pp. 455–465, 2019, doi: 10.1007/978-981-13-2553-3_44.

[39] Z. Ali, Z. M. Abdullah, B. A. Naser, R. W. Daoud, and A. H. Ahmed, "Design of a Single-Phase Inverter for Solar Energy Conversion System," NTU Journal of Renew*able Energy*, *vol. 1*, *n*o. 1, pp. 38–42, Sep. 2021. https://doi.org/10.56286/ntujre.v1i1.13.

[40] M. M. Rashid, M. A. Sharif, and F. Korkmaz, "Effects of Weather and Environmental Conditions on the Power Productivity of Photovoltaic Module in Kirkuk City," NTU Journal of Renewable Energy, vol. 4, no.1, pp. 1–6, 2023. https://doi.org/10.56286/ntujre.v4i1.

[41]Mohib A. Qasim and Thamir H. Atyia, " Evaluating the Impact of Weather Conditions on the Effectiveness and Performance of PV Solar Systems and Inverters,", NTU Journal of Renewable Energy, vol. 5, no. 1, pp. 34–46, Aug. 2023. DOI: https://doi.org/10.56286/ntujre.v5i1

[42] Bilal A. Nasir**,"** Efficiency Assessment of an Inverter based on Solar PV Energy in Baghdad City.", Engineering, Technology & Applied Science Research, Vol. 14, No. 2, pp. 13425-13429, 2024. https://etasr.com/index.php/ETASR/article/view/6948/3532.

[43] Bilal Abdullah Nasir," Determination of the Harmonic Losses in an Induction Motor Fed by an Inverter,", Engineering, Technology & Applied Science Research, Vol. 12, No. 6, 2022, 9536-9545, 2022.

[44] Bilal Abdullah Nasir," An Accurate Determination of Induction Machine Equivalent Circuit Components,", IMDC-SDSP 2020, June 28-30, 2020. DOI 10.4108/eai.28-6-2020.2297941

[45] Bilal Abdullah Nasir and Zaki Majeed Abdullah," Performance prediction of D.C motor controlled by thyristor Chopper", *AIP Conf. Proc.* 2885, 070002, 2024. https://doi.org/10.1063/5.0181947